Study of 2-D Coordinate Calibration Method for Machine Vision Systems Using Regression Analysis

Ngoc-Vu Ngo

Faculty of Mechanical Engineering, Thai Nguyen University of Technology (TNUT), No. 666, Street 3-2, Tich Luong Ward, Thai Nguyen, Vietnam
Email: ngocvu@tnut.edu.vn

***Abstract*—This paper investigates a two-Dimensional (2-D) coordinate calibration method, specifically, the quadratic transformation for machine vision systems integrated with robot arms. The objective is to establish a precise relationship between image coordinates and the world coordinate system, enabling data from the world coordinates to be used for robot arm manipulation. The calibration process was performed using a pattern target featuring 13 black circles along the OX-direction and 12 black circles along the OY-direction, each with a radius of 10 mm. The distances between the centers of the circles were 22 mm in the OX-direction and 16 mm in the OY-direction. Image processing and machine vision techniques were employed to determine the image coordinates of these calibration points. The calibration results showed that the positive maximum deviation is 0.656 mm and 0.648 mm in the OX-direction and OY-direction, respectively. The negative maximum deviation is −0.690 mm and −0.660 mm in the OX-direction and OY-direction, respectively. The experimental results demonstrate that the proposed method is both effective and accurate in determining object positions within real-world coordinates, supporting precise robot arm manipulation.**

***Keywords*—coordinate calibration, image processing, machine vision, two Dimension (2-D), robot arm**

I. Introduction

Machine vision technology utilizes illumination, image processing, and blobs analysis to extract features and positions of objects. This technology finds application in various fields, including quality inspection, optical measurement systems [1, 2], industrial automation [3], electronic semiconductors [4, 5], medical imaging [6, 7], defect inspection [8–11], and more. In manufacturing and industry, machine vision is also employed for non-contact precision measurement.

In a study by Ngo *et al.* [12], a machine vision system was developed for non-contact measurement of three-Dimensional (3-D) sizes. The study utilized a 6-point calibration algorithm to transform image coordinates into world coordinates. Image data from dual CMOS cameras was processed on a computer to measure the sizes of parts. The system demonstrated fast and accurate size determination. Importantly, it was found to be user-friendly and operationally simple. The study by Ali *et al.* [13] is highly valuable for improving precision measurement. Their proposed system aims to measure gear profiles, providing a safer alternative to traditional methods that may pose dangers during the measurement process. Additionally, existing methods are often either time-consuming or expensive. Experimental results from the proposed system were compared with those from existing systems, demonstrating significant advantages in practical applications. In a study by Rejc *et al.* [14], the authors measured the dimensions of a protector using an automated visual inspection system. They employed both linear and polynomial approximations to define the edges of selected structures of the protector. Pixel-to-metric unit transformation was achieved using a higher-order polynomial approximation. The measurement accuracy of the proposed system is within the range of ±0.02 mm, with a measurement time of less than a second. However, it cannot replace the current measurement system and can only be used in the company testing laboratory. In a study by Martínez *et al.* [15], a quality inspection system for machined metal parts was presented, utilizing an image fusion technique. The machine vision system is capable of detecting flaws on textured surfaces effectively, with a low rate of false rejections.

Calibration work within a machine vision system is crucial, as its performance relies on the accuracy of the calibration process. Shin *et al.* [16] proposed a new calibration method for a multi-camera setup using a wand dance procedure. This method initially estimates the calibration for the 3-D frame parameters using the Direct Linear Transformation (DLT) method. Subsequently, the parameters estimated in the first step are iteratively improved through nonlinear optimization using the wand dance procedure. Experimental results demonstrate that the proposed calibration method shows great promise in increasing the overall accuracy of the DLT algorithm and providing better user convenience. Ji *et al.* [17] proposed an automatic calibration method for a camera sensor

Manuscript received March 1, 2025; revised April 16, 2025; accepted August 1, 2025; published December 19, 2025.

network using 3-D texture map information of the environment provided in their research. They introduced a new image descriptor based on quantized line parameters in the Hough space (QLH) to facilitate a particle filter-based matching process between line features and the 3-D texture map information. In a study by Deng *et al.* [18], a relationship model for camera calibration was investigated. This study considered the geometric parameters and lens distortion effects of the camera. The results demonstrate that the proposed algorithm has the ability to avoid local optima and accurately complete visual identification tasks. In a study by Chuang *et al.* [19], a geometry-based camera calibration technique was presented. The proposed method is based on a closed-form solution using principal lines, where their intersection defines the principal point. Each principal line effectively represents the relative orientation or position between the image plane and the calibration pattern coordinate systems. Experimental results demonstrated the robustness and flexibility of the proposed approach. In another study, Li *et al.* [20] proposed a 3D reconstruction-based robot line-laser hand–eye calibration method. This method combines point cloud registration with a newly defined error index that more intuitively reflects calibration accuracy compared to traditional techniques. Experimental results showed that the Root Mean Square Error (RMSE) of the reconstructed point cloud reached 0.1256 mm. Jin *et al.* [21] introduced a novel representation called perspective fields, which model the local perspective properties of an image. Their study trained a neural network to predict these perspective fields, which can then be easily converted into calibration parameters. Experimental results demonstrated the robustness of this approach under various scenarios when compared to conventional camera calibration methods and highlighted its applications in image compositing. In a study by Yang *et al.* [22], an efficient initial value estimation method for matching speckle control points using Digital Image Correlation (DIC) was proposed. This method is based on perspective transformation. Experimental results confirmed that the proposed approach delivers higher calibration accuracy compared to traditional methods using chessboard or circular marker arrays. In a recent study, Ngoc and Van [23] developed an automatic measurement and classification system for a robotic arm using experimental data to build the relationship between image coordinate and the world coordinate. And the world coordinates of components are accurately determined and utilized for the manipulation of the robotic arm. This system proves to be effective and easy to use.

We can observe that machine vision technology has been widely applied across various fields, particularly in industrial automation. It offers effective solutions to enhance both operational flexibility and measurement accuracy in numerous applications. Therefore, this study presents an investigation into coordinate calibration methods for robot arms.

II. Experimental System

To investigate coordinate calibration method for a machine vision system, this study utilized a Logitech C525 CMOS camera connected to a computer via USB port. The specifications of the camera are provided in Table I. The computer was equipped with image processing and machine vision software. A calibration pattern was used to establish the relationship between image coordinates and world coordinates. The calibration pattern, depicted in Fig. 1, features 156 black circles with a diameter of 10 mm, spaced 22 mm apart in the OX-direction and 16 mm in the OY-direction. Experiments were conducted under controlled lighting conditions which is a backlighting source using diffuse white LED lighting to minimize shadows. The experimental system is illustrated in Fig. 1.

TABLE I. Specifications of the C525 Camera

No.	Specifications
1	HD video calling (1280×720 pixels) with recommended system
2	HD video capture: Up to 1280×720 pixels
3	Logitech Fluid Crystal™ Technology
4	Autofocus
5	Photos: Up to 8 megapixels
6	Hi-Speed USB 2.0 certified
7	Lens and Sensor Type: Plastic

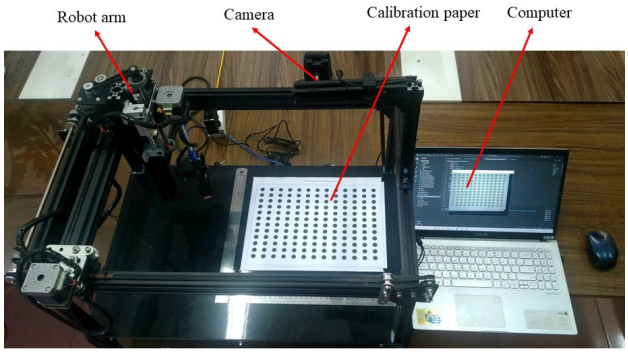

Fig. 1. Experiment system.

III. Research Methodology

A. Coordinate Calibration Using Camera Calibration

Camera calibration is essential for making accurate measurements using cameras in the real space. This is crucial because scenes are not only three-dimensional but also physical spaces with measurable units. Therefore, establishing the relationship between camera pixels and real-world units is a critical component in reconstructing a three-dimensional scene.

The camera calibration process provides both a geometric model of the camera and a lens distortion model. To complete the calibration process, both extrinsic and intrinsic parameters must be determined.

Intrinsic parameters include focal lengths in different directions, the skew between the two image axes, and the principal point and extrinsic parameters consist of the rotation matrix and translation vector.

Once the camera is calibrated, the relationship between image coordinates and world coordinates is established.

B. Coordinate Calibration Using the Perspective Transformation Method

In this method, the relationship between image coordinates and world coordinates is established using a perspective transformation model. As illustrated in Fig. 2, the camera coordinates (c_h) are determined as follows:

$$c_h = PCRGw_h \tag{1}$$

where, P is the perspective transformation matrix, C and G are the coordinate system translation matrices, R is the coordinate system rotation matrix and w_h is the world coordinates matrix. When the camera coordinate system coincides with the selected world coordinate system, the image coordinates can be calculated using the following formula:

$$c_h = Pw_h \tag{2}$$

With this method, it is necessary to determine parameters such as X_0, Y_0, Z_0, and r, as shown in Fig. 2. θ and α are the rotation angles around the OZ and OX axes, respectively, used to align the ox axis with the OX axis and the OZ axis with the OZ axis. This process is complex and time consuming.

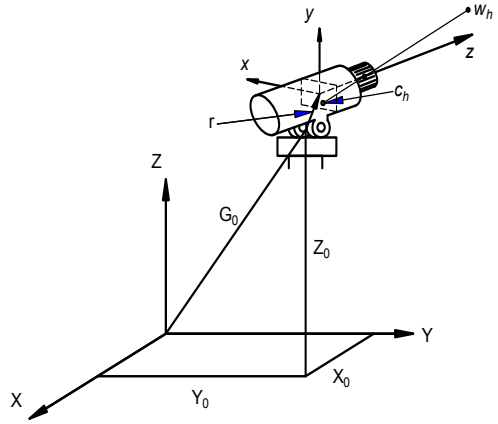

Fig. 2. Perspective transformation model.

C. Coordinate Calibration Using Quadratic Transformation and Least Square Method

To overcome the above difficulties while still ensuring the necessary accuracy for the integrated robot vision system, the quadratic transformation and least squares method are used. In this approach, the relationship between the image coordinates and the world coordinates can also be determined through transformation methods.

In this study, a quadratic transformation using regression analysis is employed to establish the relationship between the image coordinates of point I (x, y) and the world coordinates of point W (X, Y). This relationship is described by Eq. (3), as follows:

$$\begin{cases} X = a_1x^2 + b_1xy + c_1y^2 + e_1x + f_1y + g_1 \\ Y = a_2x^2 + b_2xy + c_2y^2 + e_2x + f_2y + g_2 \end{cases} \tag{3}$$

here, a_1, b_1, c_1, e_1, f_1, g_1 and a_2, b_2, c_2, e_2, f_2, g_2 represent the transformation factors. After completing the conversion of the X and Y coordinates between the world coordinate system and the image coordinate system, the least squares method is applied, as shown in Eq. (4):

$$\begin{cases} S_X = \sum_{i=1}^{n}[X - (a_1x_i^2 + b_1x_iy_i + c_1y_i^2 + e_1x_i + f_1y_i + g_1)]^2 \\ S_Y = \sum_{i=1}^{n}[Y - (a_2x_i^2 + b_2x_iy_i + c_2y_i^2 + e_2x_i + f_2y_i + g_2)]^2 \end{cases} \tag{4}$$

where S_x and S_y represent the sum of squared errors with respect to the X and Y coordinates, respectively. To determine the transformation coefficients, we compute the partial derivatives of S_x and S_y with respect to each transformation coefficient from Eq. (4), as follows:

$$\frac{\partial S_X}{\partial a_1} = 0;\ \frac{\partial S_X}{\partial b_1} = 0;\ \frac{\partial S_X}{\partial c_1} = 0;\ \frac{\partial S_X}{\partial e_1} = 0;\ \frac{\partial S_X}{\partial f_1} = 0;\ \frac{\partial S_X}{\partial g_1} = 0$$

$$\frac{\partial S_Y}{\partial a_2} = 0;\ \frac{\partial S_Y}{\partial b_2} = 0;\ \frac{\partial S_Y}{\partial c_2} = 0;\ \frac{\partial S_Y}{\partial e_2} = 0;\ \frac{\partial S_Y}{\partial f_2} = 0;\ \frac{\partial S_Y}{\partial g_2} = 0$$

D. Coordinate Calibration Process

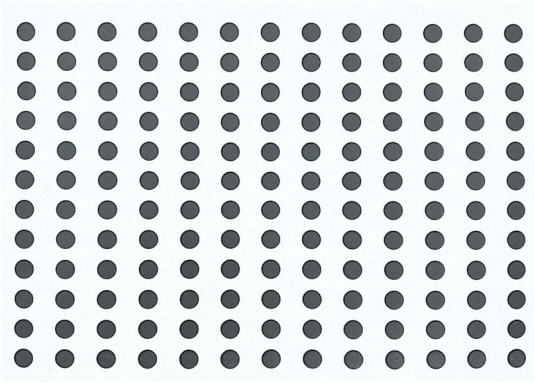

Fig. 3. Calibration pattern.

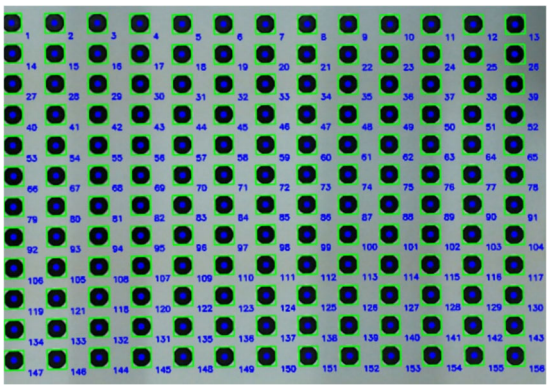

Fig. 4. Calibration result.

In this study, a CMOS camera mounted above the working platform was used to capture images of the calibration pattern, and the acquired image data was transmitted to a computer for processing. To extract the calibration markers in the calibration pattern, as shown in Fig. 3, the image was first converted to HSV color space. A color-based thresholding operation using the cv2.inRange function with lower bounds [10, 0, 100] and upper bounds [250, 250, 250] was performed to segment regions corresponding to the expected color of the circular

markers. The resulting binary mask was inverted using cv2.bitwise_not function to highlight the target objects while suppressing the background. Subsequently, the cv2.findContours function with the cv2.RETR_EXTERNAL and cv2.CHAIN_APPROX_SIMPLE modes was used to extract only the external contours of all objects, which is suitable for isolated circular markers. Among these, only the contours with an area between 500 and 2000 pixels are retained in order to eliminate noise and irrelevant objects. Then, the centers and image coordinates of all circles on the calibration pattern are identified. These centers are then sequentially labeled and ordered from the 1st to the 156th, as shown in Fig. 4. The image coordinates, along with the corresponding world coordinates (illustrated in Tables II and III), are used to compute the transformation coefficients in Eq. (3). Finally, the relationship between the world and image coordinates is established, completing the calibration process.

TABLE II. IMAGE COODINATES AND CORRESPONDING WORLD COODINATES

Point No.	The world coordinate (mm)		Image coordinate (Pixel)	
	X	*Y*	*x*	*y*
1	0	0	495	229
2	22	0	578	235
3	44	0	660	239
4	66	0	742	244
5	88	0	823	248
6	110	0	903	252
7	132	0	983	256
8	154	0	1063	260
9	176	0	1141	264
10	198	0	1219	267
11	220	0	1297	271
12	242	0	1376	273
13	264	0	1455	276
14	0	16	494	289
15	22	16	577	294
…	…	…	…	…
142	242	160	1338	834
143	264	160	1413	837
144	0	176	479	868
145	22	176	561	869
146	44	176	641	870
147	66	176	721	871
148	88	176	798	873
149	110	176	876	874
150	132	176	953	875
151	154	176	1029	878
152	176	176	1106	881
153	198	176	1182	884
154	220	176	1258	886
155	242	176	1334	888
156	264	176	1409	890

TABLE III. CALIBRATION RESULT AND DEVIATION

Point No.	Calibration coordinate (mm)		Original coordinate (mm)		Calibration deviation (mm)	
	X	*Y*	*X*	*Y*	*ΔX*	*ΔY*
1	−0.3995	−0.52593	0	0	0.399	0.526
2	21.767	−0.02895	22	0	0.233	0.029
3	43.799	−0.04802	44	0	0.201	0.048
4	65.982	0.20265	66	0	0.018	−0.202
5	88.025	0.20081	88	0	−0.025	−0.201
6	109.93	0.21384	110	0	0.070	−0.213
7	131.97	0.22847	132	0	0.030	−0.228
8	154.15	0.2447	154	0	−0.150	−0.245
9	175.91	0.28935	176	0	0.090	−0.289
10	197.77	0.061953	198	0	0.230	−0.062
11	219.78	0.1091	220	0	0.220	−0.109
12	242.16	−0.40654	242	0	−0.160	0.407
13	264.69	−0.64772	264	0	−0.690	0.648
14	−0.3421	15.473	0	16	0.342	0.527
15	21.896	15.763	22	16	0.104	0.237
…	…	…	…	…	…	…
142	242.37	160.23	242	160	−0.370	−0.230
143	264.37	160.51	264	160	−0.370	−0.510
144	−0.6223	176.66	0	176	0.622	−0.660
145	21.847	176.37	22	176	0.153	−0.370
146	44.092	176.09	44	176	−0.092	−0.090
147	66.464	175.8	66	176	−0.464	0.200
148	88.13	175.83	88	176	−0.130	0.170
149	110.19	175.55	110	176	−0.190	0.450
150	132.08	175.38	132	176	−0.080	0.620
151	153.83	175.6	154	176	0.170	0.400
152	176	175.92	176	176	0	0.080
153	197.99	176.24	198	176	0.010	−0.240
154	220.09	176.26	220	176	−0.090	−0.260
155	242.3	176.29	242	176	−0.300	−0.290
156	264.34	176.31	264	176	−0.340	−0.310

IV. RESULTS AND DISCUSSION

A. Regression Equations and Calibration Deviation

By employing regression analysis, the transformation factors (a_1, b_1, c_1, e_1, f_1, g_1 and a_2, b_2, c_2, e_2, f_2, g_2) in Eq. (3) can be determined, as shown in Eq. (5) below:

$$\begin{cases} X = 0.0000097x^2 + 0.000016xy + 0.000001y^2 + 0.25253x - 0.00316y - 128.93 \\ Y = -0.0000004x^2 + 0.000009xy + 0.000018y^2 - 0.01504x + 0.25212y - 52.78 \end{cases} \tag{5}$$

This regression model was chosen because it provides a good trade-off between model complexity and accuracy. It allows for compensation of lens distortion and planar irregularities. The coefficients were determined using least squares fitting over 156 calibration points.

From Eq. (5), the relationship between the image coordinates (x, y) and the world coordinates (X, Y) can be established. The error analysis results are depicted in Fig. 5. These results indicate that the positive maximum deviation is 0.656 mm and 0.648 mm in the OX-direction and OY-direction, respectively. The negative maximum deviation is −0.690 mm and −0.660 mm in the OX-direction and OY-direction, respectively. The calibration deviation falls within an acceptable range for the robot arm's gripper operation.

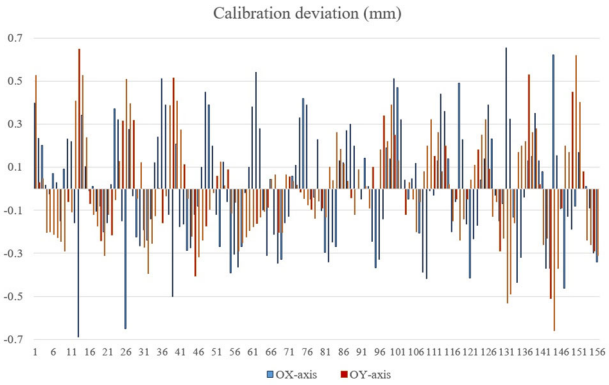

Fig. 5. Calibration deviation diagram.

B. Determining Position of Objects in Workspace

In this study, seventeen objects were utilized, consisting of nine bolts and eight nuts, as a case study to determine their positions in the work-space. Initially, all objects were recognized and labeled using the bounding box method, and then the image coordinates of their centers were then obtained using the moments funtion, as depicted in Fig. 6. Subsequently, the quadratic transformation method using regression analysis was employed to determine the world coordinates, and the results are presented in Table IV. These world coordinates will be transmitted to the robot arm for manipulation.

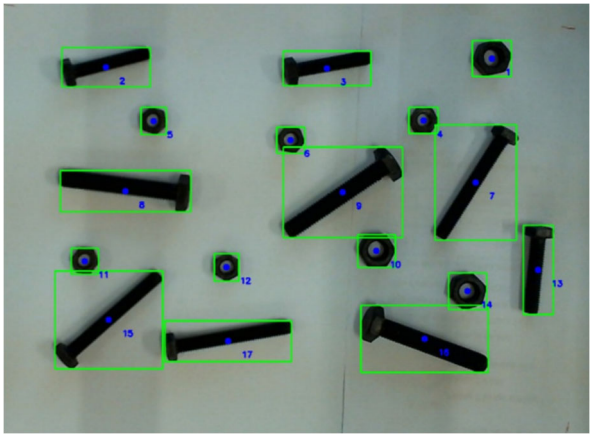

Fig. 6. Recognized objects.

TABLE IV. POSITIONS OF OBJECTS IN WORK-SPACE

No.	Objects	*x* (Pixel)	*y* (Pixel)	*X* (mm)	*Y* (mm)
1	Nut	1434	330	259.809	14.600
2	Bolt	723	346	61.768	27.991
3	Bolt	1130	348	174.146	23.477
4	Nut	1308	444	226.089	48.039
5	Nut	811	445	86.853	54.084
6	Nut	1063	480	157.383	60.966
7	Bolt	1404	558	255.871	79.293
8	Bolt	759	574	73.889	90.566
9	Bolt	1159	576	186.030	87.026
10	Nut	1221	684	205.624	117.387
11	Nut	684	703	54.439	127.731
12	Nut	945	714	127.538	128.567
13	Bolt	1519	719	262.846	124.786
14	Nut	1389	758	255.676	137.408
15	Bolt	728	811	67.780	158.343
16	Bolt	1310	846	234.450	164.004
17	Bolt	948	850	130.297	167.991

V. CONCLUSIONS AND FUTURE WORK

This study explored the use of the quadratic transformation method to derive general equations for converting image coordinates to world coordinates in two dimensions for a machine vision system integrated with a robot arm. The transformation coefficients were established using calibration pattern and regression analysis. The calibration results were then applied to determine the positions of objects, such as bolts and nuts, in the world coordinate system for manipulation by the robot arm. The findings demonstrate that the calibration deviation is acceptable for object manipulation using the robot arm's electrical gripper. Additionally, the calibration methods are simple and easy to implement.

Although the proposed method enables rapid determination of the relationship between world coordinates and image coordinates, its calibration accuracy is highly dependent on the lighting environment and camera resolution. Accurate identification of the image coordinates of the circle center on the calibration pattern is particularly critical. Therefore, future work will focus on improving the robustness and accuracy of the system. This includes employing higher-resolution cameras, implementing controlled and uniform lighting environments, and exploring advanced calibration techniques.

CONFLICT OF INTEREST

The author declares no conflict of interest.

ACKNOWLEDGMENT

The work described in this paper was supported by Thai Nguyen University of Technology (TNUT), Thai Nguyen, Vietnam.

REFERENCES

[1] R. Xiang, W. He, X. Zhang, D. Wang, and Y. Shan, "Size measurement based on a two-camera machine vision system for the bayonets of automobile brake pads," *Measurement*, vol. 122, pp. 106–116, 2018.

[2] M. K. Balasundaram and M. M. Ratnam, "In-process measurement of surface roughness using machine vision with sub-pixel edge detection in finish turning," *Int. J. Precis. Eng. Manuf.*, vol. 15, no. 11, pp. 2239–2249, 2014.

[3] A. Mishra, I. A. Sainul, S. Bhuyan, S. Deb, D. Sen, and A. K. Deb, "Development of a flexible assembly system using industrial robot with machine vision guidance and dexterous multi-finger gripper," in *Precision Product-Process Design and Optimization*, Singapore: Springer, 2018, pp. 31–71.

[4] K. Stone, A. Cintron-Aponte, and B. Simons, "Automated model-based inspection system for screening electronic components," U.S. Patent Application 15/288, 245, 2018.

[5] S. H. Huang and Y. C. Pan, "Automated visual inspection in the semiconductor industry: A survey," *Comput. Ind.*, vol. 66, pp. 1–10, 2015.

[6] D. Najrabi, M. Hamghalam, and A. Ayatollahi, "Diagnosis of astrocytoma and globalastom using machine vision," in *Proc. 2018 6th Iranian Joint Congr. Fuzzy Intell. Syst. (CFIS)*, 2018, pp. 152–155.

[7] M. Možina, D. Tomaževič, F. Pernuš, and B. Likar, "Automated visual inspection of imprint quality of pharmaceutical tablets," *Mach. Vis. Appl.*, vol. 24, no. 1, pp. 63–73, 2013.

[8] V. Chauhan and B. Surgenor, "Fault detection and classification in automated assembly machines using machine vision," *Int. J. Adv. Manuf. Technol.*, vol. 90, no. 9–12, pp. 2491–2512, 2017.

[9] G. S. Kumar, U. Natarajan, and S. S. Ananthan, "Vision inspection system for the identification and classification of defects in MIG welding joints," *Int. J. Adv. Manuf. Technol.*, vol. 61, no. 9–12, pp. 923–933, 2012.

[10] C. K. Huang, C. W. Liao, A. P. Huang, and Y. S. Tarng, "An automatic optical inspection of drill point defects for micro-drilling," *Int. J. Adv. Manuf. Technol.*, vol. 37, no. 11–12, pp. 1133–1145, 2008.

[11] C. Park, S. Choi, and S. Won, "Vision-based inspection for periodic defects in steel wire rod production," *Opt. Eng.*, vol. 49, no. 1, 017202, 2010.

[12] N. V. Ngo, Q. C. Hsu, W. L. Hsiao, and C. J. Yang, "Development of a simple three-dimensional machine-vision measurement system

for in-process mechanical parts," *Adv. Mech. Eng.*, vol. 9, no. 10, pp. 1–11, 2017.
[13] M. H. Ali, S. Kurokawa, and K. Uesugi, "Camera based precision measurement in improving measurement accuracy," *Measurement*, vol. 49, pp. 138–147, 2014.
[14] J. Rejc, F. Kovačič, A. Trpin, I. Turk, M. Štrus, D. Rejc, and M. Munih, "The mechanical assembly dimensional measurements with the automated visual inspection system," *Expert Syst. Appl.*, vol. 38, no. 8, pp. 10665–10675, 2011.
[15] S. S. Martínez, C. O. Vázquez, J. G. García, and J. G. Ortega, "Quality inspection of machined metal parts using an image fusion technique," *Measurement*, vol. 111, pp. 374–383, 2017.
[16] K. Y. Shin and J. H. Mun, "A multi-camera calibration method using a 3-axis frame and wand," *Int. J. Precis. Eng. Manuf.*, vol. 13, no. 2, pp. 283–289, 2012.
[17] Y. Ji, A. Yamashita, and H. Asama, "Automatic calibration of camera sensor networks based on 3D texture map information," *Robot. Auton. Syst.*, vol. 87, pp. 313–328, 2017.
[18] L. Deng, G. Lu, Y. Shao, M. Fei, and H. Hu, "A novel camera calibration technique based on differential evolution particle swarm optimization algorithm," *Neurocomputing*, vol. 174, pp. 456–465, 2016.
[19] J. H. Chuang, C. H. Ho, A. Umam, H. Y. Chen, J. N. Hwang, and T. A. Chen, "Geometry-based camera calibration using closed-form solution of principal line," *IEEE Trans. Image Process.*, vol. 30, pp. 2599–2610, 2021.
[20] M. Li, Z. Du, X. Ma, W. Dong, and Y. Gao, "A robot hand-eye calibration method of line laser sensor based on 3D reconstruction," *Robot. Comput.-Integr. Manuf.*, vol. 71, 102136, 2021.
[21] L. Jin, J. Zhang, Y. Hold-Geoffroy, O. Wang, K. Blackburn-Matzen, M. Sticha, and D. F. Fouhey, "Perspective fields for single image camera calibration," in *Proc. IEEE/CVF Conf. Comput. Vis. Pattern Recognit.*, 2023, pp. 17307–17316.
[22] X. Yang, X. Chen, and J. Xi, "Perspective transformation based-initial value estimation for the speckle control points matching in an out-of-focus camera calibration using a synthetic speckle pattern," *Opt. Express*, vol. 30, no. 2, pp. 2310–2325, 2022.
[23] V. N. Ngoc and C. D. Van, "Development of an automatic measurement and classification system for a robotic arm using machine vision," *Int. J. Mech. Eng. Robot. Res.*, vol. 13, no. 4, pp. 489–494, 2024.